Analytica Chimica Acta 1155 (2021) 338351

Contents lists available at ScienceDirect

Analytica Chimica Acta

journal homepage: www.elsevier.com/locate/aca

Simple, rapid, and sensitive on-site detection of Hg^{2+} in water samples through combining portable evanescent wave optofluidic biosensor and fluorescence resonance energy transfer principle

Yue Zhou [a, 1], Hongliang Wang [b, 1], Dan Song [b], Zhanguo Li [a], Shitong Han [a], Feng Long [b, **], Anna Zhu [a, *]

[a] State Key Laboratory of NBC Protection for Civilian, Beijing, 102205, China
[b] School of Environment and Natural Resource, Renmin University of China, Beijing, 100872, China

HIGHLIGHTS

- Portable evanescent wave optofluidic biosensor (EWOB) was developed for simple sensitive detection of Hg^{2+}.
- The influence of several key environmental factors on Hg^{2+} biosensor, such as pH, temperature, and ionic strength, was in details investigated to be practical in the field.
- A detection cycle for a single sample, including the measurement and regeneration, was under 10 min with a Hg^{2+} detection limit of 8.5 nM.
- The EWOB has several advantages including high sensitivity and selectivity, portability, short assay time, easy-to-operation, cost-effectiveness, and robustness.
- The EWOB is also potentially applicable to detect other heavy metal ions or small molecule targets for which DNA/aptamers could be applied as specific biosensing probes.

GRAPHICAL ABSTRACT

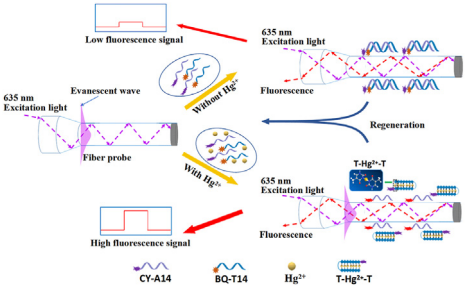

ARTICLE INFO

Article history:
Received 8 January 2021
Received in revised form
17 February 2021
Accepted 23 February 2021
Available online 25 February 2021

ABSTRACT

Rapid and sensitive detection of Hg^{2+} in the environment and drinking water is vital because of its non-degradability, bioaccumulation, and high toxicity. Herein, we report a portable evanescent wave optofluidic biosensor (EWOB) for simple sensitive detection of Hg^{2+} using fluorescence labeled poly-A DNA strand (CY-A14) and quencher labeled poly-T DNA strand (BQ-T14) as signal reporter and biorecognition element, respectively. Both CY-A14 and Hg^{2+} can competitively bind with BQ-T14 based on DNA hybridization and the specifical binding of Hg^{2+} and T bases of DNA to form T-Hg^{2+}-T mismatch structure, respectively. Higher concentration of Hg^{2+} lead to less CY-A14 bound to BQ-T14 and thus a higher

* Corresponding author.
** Corresponding author.
E-mail addresses: longf04@ruc.edu.cn (F. Long), chuanna0306@163.com (A. Zhu).
[1] These authors have equal contribution to this work.

https://doi.org/10.1016/j.aca.2021.338351

Keywords:
Mercury ions
Evanescent wave fluorescence
Fluorescence resonance energy transfer
DNA
Optofluidic biosensor

fluorescence intensity. The influence of several key environmental factors on Hg^{2+} biosensor, such as pH, temperature, and ionic strength, was investigated in details because they were essential for practical applications of Hg^{2+} biosensor. Under optimal conditions, a detection cycle for a single sample, including the measurement and regeneration, was less than 10 min with a Hg^{2+} detection limit of 8.5 nM. The high selectivity of the biosensor was showed by evaluating its response to various potentially interfering metal ions. Our results clearly demonstrated that the portable EWOB could serve as a powerful tool for rapid and sensitive on-site detection of Hg^{2+} in real water samples. The EWOB is also potentially applicable to detect other heavy metal ions or small molecule targets for which DNA/aptamers could be applied as specific biosensing probes.

1. Introduction

Mercury ions (Hg^{2+}) can cause severe health problems such as organic damages, growth or mental retardation, cancers, and even death because of its non-degradability, bioaccumulation, and high toxicity [1–7]. A major source of Hg^{2+} exposure originates from the contaminated drinking water and aquatic food [8]. Traditional Hg^{2+} detection methods include atomic absorption spectrometry (AAS), inductively coupled plasma (ICP), and atomic fluorescence spectrometry (AFS). However, these methods have several limitations, such as expensive instrumentation, complicated sample preparation, high cost, and time-consuming [9–12]. Therefore, it is vital to develop rapid, sensitive, and easy-to-operation Hg^{2+} detection technologies to protect the public, especially for developing countries and resource-limited areas.

Biosensors have attracted tremendous interest owing to their distinctive simplification, rapidity, sensitivity, and specificity [13–15]. Since Ono et al. reported the ability of Hg^{2+} to specifically bind to thymine-thymine (T-T) mismatch structure to form thymine-Hg^{2+}-thymine (T-Hg^{2+}-T) complexes [16], many Hg^{2+} biosensors based on colorimetric, electrochemical, and optical transducer have been constructed for sensitive detection of Hg^{2+}. However, challenges still remain in how to simplify complicated design and operation to afford rapid and sensitive on-site detection of Hg^{2+}. To date, most researches focused on the design of Hg^{2+} detection strategies [17–20], and little attention was put on the influences of environmental factors to T-Hg^{2+}-T mismatch structure-based biosensors. As we well known, several environmental factors including pH, temperature, and ion strength had significant influences on DNA hybridization efficiency, which was unavoidable to impact the formation of T-Hg^{2+}-T mismatch structure as well as accuracy of Hg^{2+} detection. Therefore, it is also essential to clarify their influencing mechanisms for in-field applications of Hg^{2+} biosensor.

Herein, we report a novel portable evanescent wave optofluidic biosensor (EWOB) for simple, rapid, and sensitive on-site detection of Hg^{2+} based on fluorescence resonance energy transfer principle. Evanescent wave optofluidic biosensors, integrating the advantages of evanescent wave fluorescence, optofluidic, and biosensor, possess several features such as high sensitivity, low background signal, immunity to electromagnetic interference, robustness, and portability for on-site measurements. To simplify the design of the Hg^{2+} biosensor, one poly-T base DNA strand labeled with quenching molecule and one poly-A base DNA strand labeled with fluorescence molecule were regarded as biorecognition element and signal reporter, respectively. Based on fluorescence resonance energy transfer principle, the sensitive detection of Hg^{2+} was realized using the EWOB because of the specific interactions between Hg^{2+} and T bases of DNA to form T-Hg^{2+}-T mismatch structure. The influencing of pH, temperature, and ion strength on the Hg^{2+} detection were investigated in details to obtain optimal detection conditions. Finally, the proposed method was applied for the simple on-site detection of Hg^{2+} in real water samples.

2. Experimental section

2.1. Materials and chemicals

Poly-T base DNA strand labeled with quenching molecule (5′-TTTT TTTT TTTT TT-BHQ3-3′, BQ-T14) and its complementary strand, poly-A base DNA strand labeled with fluorescence molecule (5′-Cy5.5-AAAA AAAA AAAA AA-3′, CY-A14), were synthesized from Shanghai biotechnology (Shanghai, China). 0.01 M 3-(N-Morpholino) propanesulfonic acid (MOPs) buffer solution (pH ≈ 6.0) was prepared. $Hg(NO_3)_2$ solution was purchased from Shanghai Macklin Biochemical Co. Ltd (Shanghai, China). A series of Hg^{2+} standard solutions were prepared by diluting stock Hg^{2+} solution using MOPs buffer. The 0.5% sodium dodecyl sulfate (SDS) with pH 1.9 was used to regenerate the fiber optic probe. Unless specified, all other chemical reagents with analytical grade were purchased from Beijing Chemical Agents.

A TG16-WS desktop high-speed centrifuge (Hunan Xiangyi Centrifuge Instrument Co. Ltd, China) and a temperature-constant mixer (Hangzhou Youning Instrument Co., Ltd, China) were used.

2.2. Design of portable EWOB and biosensing mechanism of Hg^{2+}

The portable EWOB was developed based on the evanescent wave all-fiber fluorescence platform previously described [21] (Fig. S1). In this platform (Fig. 1A), a 635-nm laser with pigtail was launched into a tapered fiber probe (Preparation method was shown in Supporting Information) through a single multi-mode fiber coupler (SMFC). The incident light transmitted in the fiber probe via total internal reflection, and the electromagnetic field extended out from the fiber probe interface into the solution because of the non-zero Fresnel transmission coefficients for the transverse electric wave and the transverse magnetic wave [22]. This electromagnetic field, named as evanescent wave, decayed exponentially with distance from the surface and was sufficient to excite molecules in close vicinity to the fiber probe surface. Part of fluorescence coupled back into the fiber probe and was detected by the EWOB.

The biosensing mechanism of Hg^{2+} detection using the EWOB is demonstrated in Fig. 1B. When no Hg^{2+} existed in the sample, CY-A14 hybridized with BQ-T14, resulting in fluorescence quenching due to FRET and few detectable fluorescence intensities. When Hg^{2+} existed in the sample, Hg^{2+} competitively bound with BQ-T14 to form a stable "T-Hg^{2+}-T" mismatch structure, resulting in that some of the CY-A14 couldn't hybrid with BQ-T14. The free CY-A14 was excited by evanescent wave generated on the surface of the fiber probe, and a relative strong fluorescence intensity was detected by the EWOB. The higher the Hg^{2+} concentration was, the

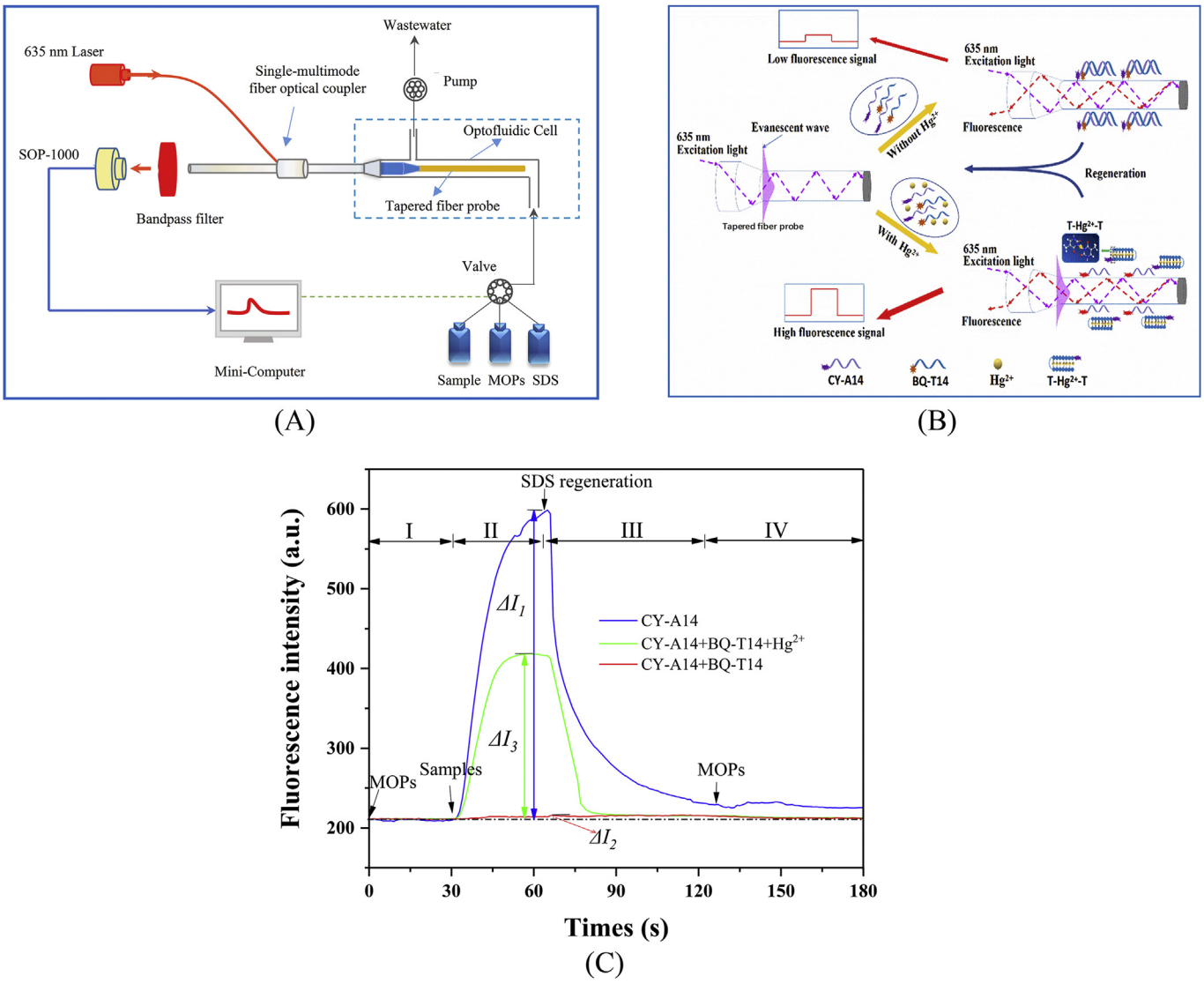

Fig. 1. Design of portable EWOB and biosensing mechanism of Hg^{2+}. (A) Schematic of portable EWOB. Its photo is shown in Supporting information. (B) Biosensing mechanism of Hg^{2+} using EWOB based on T-Hg^{2+}-T mismatch structure and FRET principle. (C) Typical signal traces of Hg^{2+} detection: Blue line, 30 nM CY-A14; Red line, the mixture of 30 nM CY-A14 and 45 nM BQ-T14; Green line, the mixture of 30 nM CY-A14, 45 nM BQ-T14 and 185 nM Hg^{2+}. (For interpretation of the references to color in this figure legend, the reader is referred to the Web version of this article.)

more free CY-A14 was, thus resulting in a higher fluorescence intensity. According to the relationship between the fluorescence intensity and the Hg^{2+} concentration, the quantitative detection of Hg^{2+} could be realized.

The detection process of the EWOB was as follows. First, a tapered fiber probe was installed in the optofluidic cell, then MOPs buffer solution was introduced over the fiber probe surface for cleaning and the baseline was obtained (Step I in Fig. 1C). Second, 50 μL CY-A14, 75 μL BQ-T14, and 75 μL different concentrations of Hg^{2+} solutions were mixed and incubated for a certain time. The mixture was injected into the optofluidic cell for detection, and the fluorescence intensity was real-time detected by the EWOB (Step II in Fig. 1C). Third, SDS solution was pumped into the optofluidic cell to regenerate the fiber probe (Step III in Fig. 1C). Finally, the fiber probe was cleaned by MOPs buffer for next detection (Step IV in Fig. 1C).

2.3. Effects of pH, temperature and ion strength on the Hg^{2+} detection

To investigate the effect of pH, MOPs with different pH (adjusted with HNO_3 or NaOH solution, and the desired pH = 2, 3, 4, 5, 6, 7, 8, 9, 11) were used to prepare CY-A14, BQ-T14 and different concentration Hg^{2+} solutions. Then, 50 μL CY-A14, 75 μL BQ-T14, and 75 μL Hg^{2+} solutions of different concentrations were mixed and incubated for 7 min. Then, the mixture was introduced into the optofluidic cell for fluorescence detection.

To investigate the effect of temperature, the mixture of CY-A14, BQ-T14, and Hg^{2+} was incubated under 15 °C, 20 °C, 26 °C, 30 °C, and 35 °C, respectively, and then their fluorescence intensities were detected by the EWOB.

To investigate the effect of ion strength, the ion strength of various solutions was adjusted with $NaNO_3$, and the mixture of CY-A14, BQ-T14 and Hg^{2+} had final ionic strength ranged from 0.05 mol/kg to 1.00 mol/kg (Table S1). After incubation, the

fluorescence intensity of the mixture was detected by the EWOB.

2.4. Mercury ion analysis

Water samples spiked by different concentrations of Hg^{2+} were mixed with CY-A14 and BQ-T14 at a fixed concentration. After incubated for 7 min, the mixture was introduced into the optofluidic cell and allowed to detect its fluorescence intensity. The fiber probe surface was then regenerated with a SDS solution (0.5%, pH 1.9) for 60 s and washed with a MOPs solution.

To evaluate potential matrix effect of environmental samples on Hg^{2+} biosensor, spiked samples of tap water, commercially available bottled water, lake water, and underground water were detected at various concentrations ranged from 75 to 185 nM. To assess the biosensor's specificity, we investigated its responses to potentially interfering metal ions such as Ca^{2+}, Zn^{2+}, Cu^{2+}, Mg^{2+}, Cd^{2+}, and Pb^{2+} at a concentration up to 3.5 μM.

3. Results and discussion

3.1. Feasibility characteristics of Hg^{2+} detection mechanism

To verify the feasibility of Hg^{2+} detection using the EWOB based on the specific interactions between Hg^{2+} and T-T mismatch structure and FRET principle. Various control experiments were performed (Fig. 1C). When free CY-A14 was introduced into the optofluidic cell, a maximum fluorescence intensity (ΔI_1) was obtained because most of the fluorescence molecules labeled on the free CY-A14 were excited by the evanescent wave and no fluorescence was quenched. Previous references demonstrated that the tapered fiber probe with a matching V number greatly enhanced the excitation and collection efficiency of the fluorescence. The fluorescence intensity was over 390 (a.u.) when the free CY-A14 was 30 nM, indicating that the EWOB had a high sensitivity for free CY-A14 using the tapered fiber probe as optical transducer. Then, few fluorescence intensities (ΔI_2) could be observed when the mixture of CY-A14 and BQ-T14 was added, indicating that CY-A14 and BQ-T14 could hybridize to form double strand structure and Cy5.5 was quenched by BHQ3 due to the FRET effect. Our results demonstrated that when the ratio of CY-A14 and BQ-T14 was 1.5, the fluorescence of CY-A14 could be well quenched by BQ-T14 (Fig. S2). OnceHg^{2+} existed in the mixture, a high fluorescence intensity (ΔI_3) was detected. This contributed to the formation of T-Hg^{2+}-T mismatch structure, which limited the hybridization between BQ-T14 and CY-A14. The free CY-A14 could be effectively excited by the evanescent wave. When CY-A14, BQ-T14 and Hg^{2+} were mixed, the detectable fluorescence intensity reached a plateau after incubation for 7 min (Fig. S3). These results confirmed that the biosensor, consisted of CY-A14 and BQ-T14, could be applied for the Hg^{2+} detection using the EWOB based on the FRET principle.

The net fluorescence intensity ΔI used for determination of dose-response curves was calculated according to Equation (1):

$$\Delta I_m = \text{Fluorescence intensity value} - \text{Baseline value} \quad (1)$$

Here, m = 1, 2 or 3.
m = 1 means the net fluorescence intensity of CY-A14
m = 2 means the net fluorescence intensity of CY-A14+BQ-T14
m = 3 means the net fluorescence intensity of CY-A14+BQ-T14 + Hg^{2+}

3.2. Effect of pH on the Hg^{2+} biosensor

Because pH affected the DNA hybridization and the formation of T-Hg^{2+}-T structure, we investigated the effect of pH on the performance of Hg^{2+} biosensor. The fluorescence intensities of free CY-A14 (ΔI_1) and the fluorescence intensities of CY-A14 + BQ-T14 (ΔI_2) under various pH conditions were regarded as the references. As expected, under low pH conditions (<3), all the fluorescence intensity of Hg^{2+} biosensor, including ΔI_1, ΔI_2 and ΔI_3, were very low (Fig. 2A). Moreover, all the ΔI_3 under such pH were almost unchanged even if 375 nM Hg^{2+} was added (Fig. 2B). Therefore, it is impossible to apply such biosensor to detect Hg^{2+} in water sample when its pH is less than 3.

In the range of pH 4–9, ΔI_2 was by far less than ΔI_1, indicating

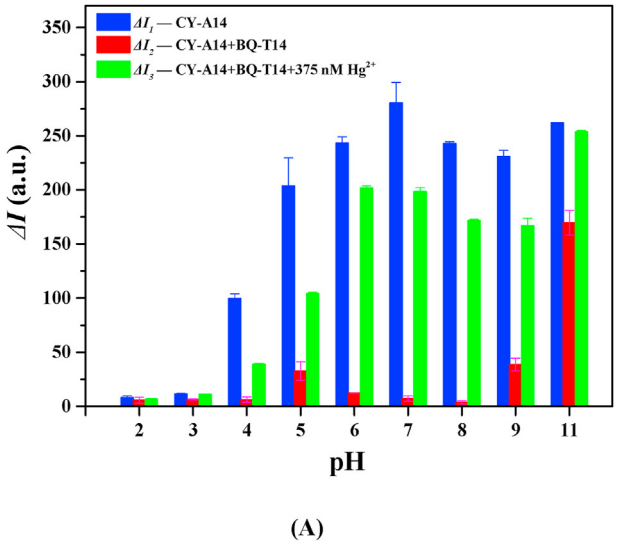

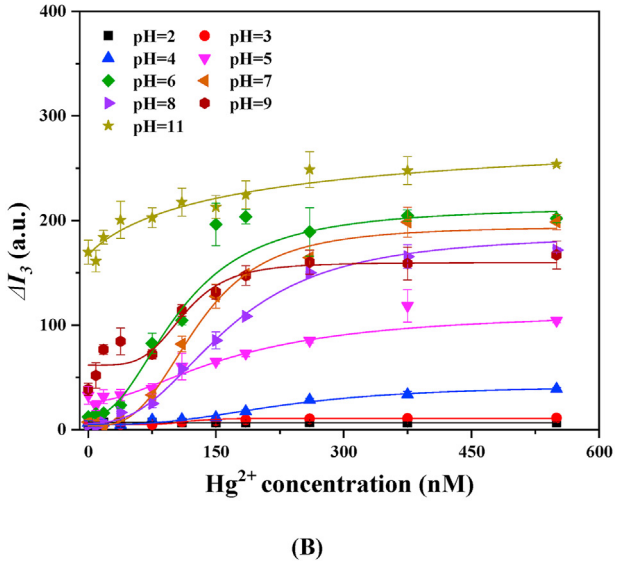

Fig. 2. Effect of pH on the Hg^{2+} biosensor. (A) Fluorescence intensity measured by the EWOB at various pH values. Experimental condition: 26 °C, $NaNO_3$ = 150 mM, and the concentration of Hg^{2+}, CY-A14 and BQ-T14 is 375 nM, 30 nM and 45 nM, respectively. (B) Dose-response curves of Hg^{2+} biosensor at different pH. The concentration of Hg^{2+} ranges from 0 to 550 nM. Error bars correspond to SD of data points for triplicate experiments (n = 3).

the fluorescence of the CY-A14 could be quenched well based on the FRET effect after incubated with BQ-T14. The ΔI_3 was high than ΔI_2, which could contribute to the formation of T-Hg^{2+}-T structures and reduced hybridization of CY-A14 and BQ-T14. The free CY-A14 were excited by the evanescent wave and the emission fluorescence was detected by the EWOB. From Fig. 3A, the fluorescence intensity ΔI_3 increases with the pH when pH is less than 6. If pH further raised, the ΔI_3 decreased. When pH was higher than 9, the fluorescence quenching efficiency was obviously degraded. Especially for pH = 11, ΔI_2 was still high, indicating that the hybridization of CY-A14 and BQ-T14 could not be formed and only part of CY-A14 was quenched. Therefore, the high pH solution was also unsuitable for the Hg^{2+} biosensor.

Studies demonstrated that thymine deprotonation could be brought about at pH 6.8, below the pH at which thymine becomes deprotonated (the pKa of the proton at N3 position of thymine is 9–10), because initial Hg^{2+} binding to O4 and/or O2 positions of the canonical tautomer of thymine can acidify the proton at the N3 position [23,24], which was coherent with our experimental phenomena obtained at pH 4–9. The ΔI_3 at various pH were different (Fig. 2B). We assumed that pH could affect the thymine deprotonation process in the formation of T-Hg^{2+}-T structure. The deprotonation could contributed to the formation of Hg–OH, and different pH might lead to different composition of $[Hg(H_2O)_x]^{2+}$ in solution, thus affecting the ΔI_3. Furthermore, we performed the dose-response experiments at various pH values. As shown in Fig. 2B, the dose-response curves of Hg^{2+} detection could be obtained when pH was ranged from 4 to 9. Obviously, the dose-response curves at pH 4, 5, and 9 could not be applied for the Hg^{2+} detection in real samples because they either had low fluorescence intensity or narrow detection range. Considering the fluorescence intensity and dynamic detection range, the suitable pH for Hg^{2+} biosensor based on T-T mismatch structure ranges in 6–8.

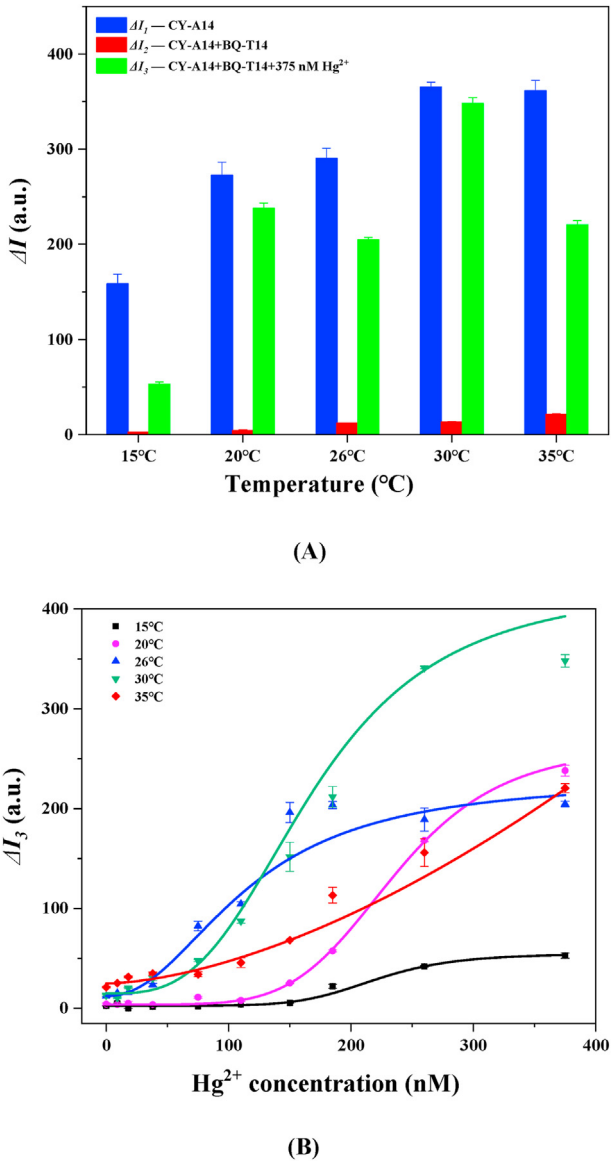

Fig. 3. Effect of temperature on the Hg^{2+} biosensor. (A) Fluorescence intensity measured by the EWOB at different temperature. Experimental condition: pH = 6, $NaNO_3$ = 150 mM, and the concentration of CY-A14, BQ-T14 and Hg^{2+} is 30 nM, 45 nM and 375 nM, respectively. **(B)** Dose-response curves of Hg^{2+} biosensor at different temperature. Testing condition: pH = 6, $NaNO_3$ = 150 mM, and the concentration of Hg^{2+} ranges from 0 to 375 nM. Error bars correspond to SD of data points for triplicate experiments (n = 3).

3.3. Effect of temperature on the Hg^{2+} biosensor

Tanaka et al. showed that the formation of T-Hg^{2+}-T structure originated from the Hg^{2+} replacing the imino protons of the residues [25]. The Hg^{2+} surrounded by structured water molecules could be dehydrated, and the protons at the N3 position of the two thymine bases in T:T might release. Then, the dehydrated Hg^{2+} bound with the two deprotonated thymine bases to form N3–Hg–N3, in which the Hg^{2+} dehydration was an entropy enhancement process [26–29]. In addition, the formation of DNA base pairs was driven by enthalpy and entropy and sensitive to the temperature. Therefore, the thermal stability and formation of the T-Hg^{2+}-T structure might be affected by the temperature.

Here, we investigated the response of Hg^{2+} biosensor to the temperature ranging in 15 °C–35 °C. As shown in Fig. 3, all the ΔI_2 are low, indicating the CY-A14 are quenched. The quenching efficiency slightly decreased with the increase of temperature. These results demonstrated that the temperature had little influence on the DNA hybridization under the experimental temperatures. It was well known that DNA hybridization dynamics was the best in the temperature range of 20 °C–25 °C [30], and high temperature might cause the hybridization difficult. The ΔI_3 exhibited a strong temperature dependence across the experimental range (15 °C–35 °C). The ΔI_3 at 15 °C was the lowest, indicating that the T-Hg^{2+}-T structure was difficult to form at such low temperature. This further verified the entropy enhancement of the Hg^{2+} dehydration. When temperature was 30 °C, the ΔI_3 was nearly the same as the ΔI_1, indicating that all the CY-A14 in the detection system were almost free. Therefore, the proper increase of temperature might be beneficial for Hg^{2+} biosensor, which promoted the dehydration of hydrated Hg^{2+} as well as the formation of the T-Hg^{2+}-T structure. However, when temperature was higher than 35 °C, the ΔI_3 decreased instead, which might contribute to that higher temperature could destroy thermal stability of the T-Hg^{2+}-T structure. Kratochvílová et al. showed that the interaction between bases would be weakened with increasing temperature, because it increased the possibility of charge transfer in a more suitable position [31]. It was consistent with our experimental results.

Fig. 3B displayed the dose-response curves at different temperatures. When temperature was between 20 °C and 30 °C, good dose-response curves could be obtained. At lower and higher temperature, the dose-response curves could not be applied for the Hg^{2+} detection in real samples because they either had low fluorescence intensity or narrow detection range. Considering the fluorescence intensity and dynamic detection range, the most

suitable temperature for Hg^{2+} biosensor based on T-T mismatch structure was 30 °C.

3.4. Effect of ion strength on the Hg^{2+} biosensor

Ion strength is one of the most important factors for Hg^{2+} biosensor because it not only determines the hybridization efficiency and stability of DNA double strands, but also affects the formation of T-Hg^{2+}-T structure. Fig. 4A shows the fluorescence intensity measured by the EWOB under ion strengths ranging in 0.05 mol/kg ~1.0 mol/kg. The ΔI_1 initially decreased and then increased with increasing the ion strengths, which might be related with electrostatic repulsion and compression of the electrostatic double layer surrounding the DNA and the silica surface. For the experimental ion strength range, all of the ΔI_2 were low, indicating that the CY-A14 hybridized well with the BQ-T14. The ΔI_2 decreased with increasing the ion strength because the increase of ion strength reduced the electrostatic repulsion between the negatively charged phosphate groups of DNA backbone, improved the flexibility of DNA, and reduced the resistance of hybridization [32–35].

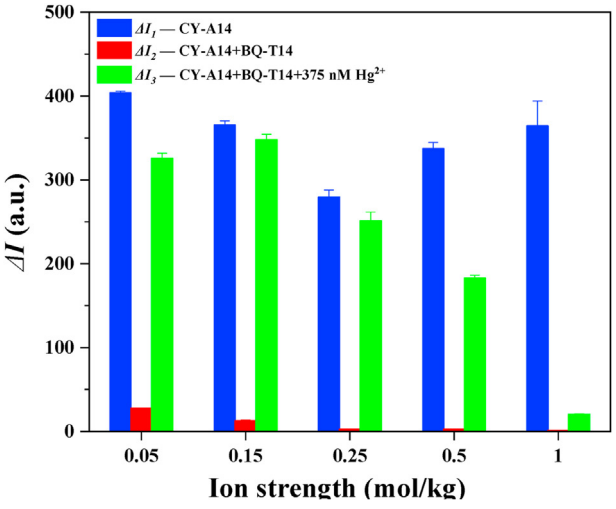

Fig. 4. Effect of ion strength on the Hg^{2+} biosensor. **(A)** Fluorescence intensity measured by the EWOB at different ion strengths. Experimental condition: 26 °C, pH = 6, and the concentration of CY-A14, BQ-T14 and Hg^{2+} is 30 nM, 45 nM and 375 nM, respectively. **(B)** Dose-response curves of Hg^{2+} biosensor at various ion strengths. The concentration of Hg^{2+} ranges from 0 to 375 nM. Error bars correspond to SD of data points for triplicate experiments (n = 3).

Although high hybridization efficiency of the CY-A14 and the BQ-T14 is important for reducing the background signal and increasing signal/noise ratio, the effective binding between the BQ-T14 and Hg^{2+} is also essential for developing a sensitive Hg^{2+} biosensor. From Fig. 4A, low ion strength is obviously conducive for the Hg^{2+} biosensor. When the ion strength was higher than 0.15 mol/kg, the ΔI_3 significantly decreased with increasing the ion strength. When the ion strength reached 1.0 mol/kg, ΔI_3 was very low even when the Hg^{2+} concentration was 375 nM, indicating that the Hg^{2+} could not compete with CY-A14 for binding with BQ-T14. To improve the detection performance of Hg^{2+} biosensor, a balance between the hybridization efficiency of DNA and the response efficiency of Hg^{2+} biosensor needed to be carefully weighed.

The above results were further confirmed by the dose-response results of Hg^{2+} biosensor at various ion strengths (Fig. 4B). When the ion strength was over 0.5 mol/kg, the responses of biosensors for different concentrations of Hg^{2+} significantly degrade, and the limit of detection increased and the dynamic detection range became narrow. If increasing the ion strength to 1.0 mol/kg, the biosensor had no response for Hg^{2+} because of too strong binding between DNA double strands. When the ionic strength was 0.15 mol/kg, the changing trend of ΔI_3 with the increase of Hg^{2+} concentration was more obvious than other ion strength conditions, indicating that the biosensor would obtain the best performance at this ion strength condition.

3.5. Dose-response curve for Hg^{2+} detection

Once the general assay parameters were optimized, quantitative analysis of Hg^{2+} was performed using the EWOB. Fig. 5A demonstrates the typical fluorescence signal traces when the mixture consisted of CY-A14, BQ-T14 and Hg^{2+} of various concentrations is introduced over the tapered fiber probe in the optofluidic cell. A test cycle, including the introduction of MOPs, the detection of fluorescence intensity of the mixture, and the fiber probe regeneration, only needed 3 min using the EWOB. One could see that with increasing Hg^{2+} concentration, the fluorescence intensity detected by the EWOB proportionally increased as expected. This contributed to that the more BQ-T14 bound with Hg^{2+} to form the T-Hg^{2+}-T mismatch structure, and the higher concentration of free CY-A14 existed in the homogenous solution. The latter was effectively excited by evanescent wave, thus resulting in a higher fluorescence intensity.

Fig. 5B shows the calibration curve for Hg^{2+} detection, which is normalized by expressing the signal of each standard point as the ratio to that of the blank sample containing no Hg^{2+}, as following.

$$SI = \Delta I_3/\Delta I_1 \quad (2)$$

The proportionally increasing fluorescence intensity as the concentration of Hg^{2+} established a dose-response curve for quantification of Hg^{2+} over a concentration range from 0 to 375 nM. The limit of detection (LOD) of 8.5 nM was obtained from the calibration curve based on a signal-to-noise ratio of 3. Therefore, this novel biosensor can directly detect Hg^{2+} in drinking water with the ability to meet even the most stringent EPA requirement (10.0 nM). The LOD is comparable to those of the other biosensors (Table S2). Compared to these biosensors, however, the proposed biosensor has several advantages. First, simple sensitive detection of Hg^{2+} can be realized by simply mixing the CY-A14, BQ-T14, and

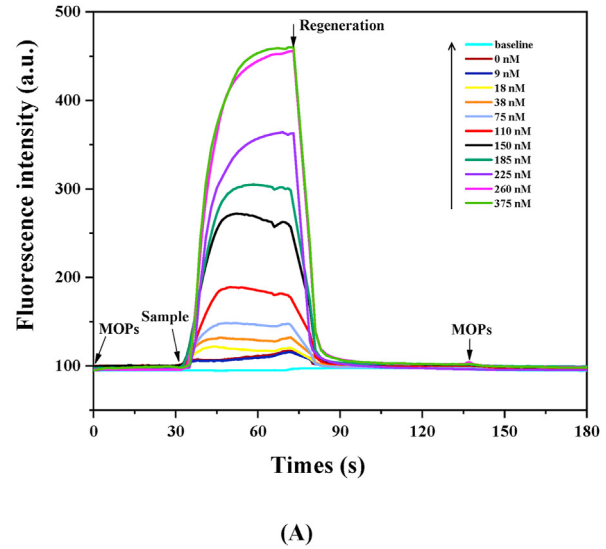

(A)

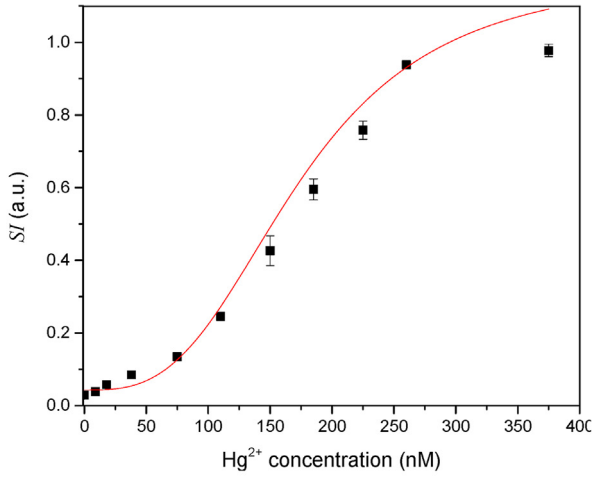

(B)

Fig. 5. (A) Typical signal curves of Hg^{2+} detection using the EWOB; (B) Dose-response curve of Hg^{2+} detection. Experimental condition: 26 °C, pH = 6, $NaNO_3$ = 150 mM, the concentration of CY-A14 and BQ-T14 is 30 nM and 45 nM respectively. The error bars corresponded to the standard deviation of the data points in three repeated experiments (n = 3).

sample and detecting its fluorescence intensity using the EWOB. Second, the complex biorecognition molecule immobilization is not required because of its homogenous detection, which generally decreases the activity of biomolecules and the sensitivity of biosensor. Third, the use of evanescent wave fluorescence platform can greatly improve the signal-to-noise ratio and reduce the effect of solution matrix due to the limited penetration depth. Fourth, the application of the synthesized CY-A14 and BQ-T14, regarded as a biorecognition element and signal reporter for Hg^{2+} detection, allows it to be as low as $ 0.05 per test. In addition, the portable EWOB is much simpler and faster (<10 min).

3.6. Selectivity of Hg^{2+} biosensor

To investigate potential interferences from other metal ions, we evaluated the sensor's response to 3.5 μM Ca^{2+}, Zn^{2+}, Cu^{2+}, Mg^{2+}, Cd^{2+}, and Pb^{2+}. As seen from Fig. 6, our biosensor exhibits high selectivity toward Hg^{2+} with no significant response to the other

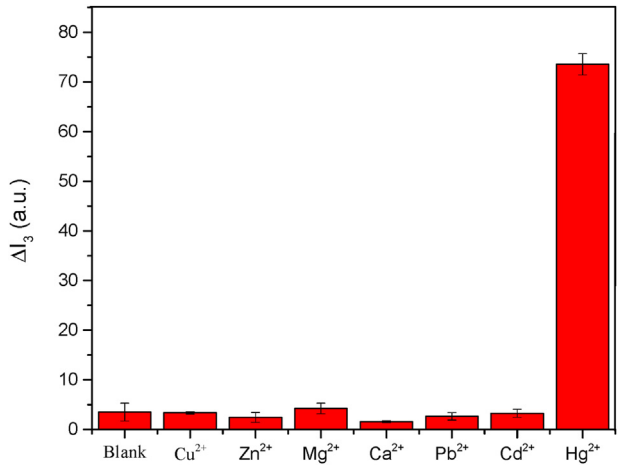

Fig. 6. Comparison of fluorescence intensity in the presence of various metal ions. The concentration of Hg^{2+} is 115 nM, and the concentration of other metal ions is 3.5 μM.

metal ions tested, although the concentrations of other metal ions are 30 times higher than that of Hg^{2+}. This selectivity contributed to the high selective binding of Hg^{2+} to T-T mismatches, which allowed the formation of stable T-Hg^{2+}-T complexes.

3.7. Environmental water samples analysis

Since the presented Hg^{2+} biosensor has demonstrated high specificity and sensitivity, we further investigated the potential application to real water samples. To evaluate possible matrix effect of water samples [36], several samples spiked with Hg^{2+} were tested using the EWOB. The water samples were tap water, bottle water, lake water, and underground water samples, and were spiked with Hg^{2+} from its stock solutions at concentrations of 75, 115, and 185 nM. These samples were detected Hg^{2+} content as described above. As shown in Table 1, the results reveal good agreement between the actual and measured Hg^{2+} concentrations. These data confirmed that the EWOB could be applicable for Hg^{2+} detection with enough precision and accuracy without significant matrix effect in real environmental samples. Although we only demonstrated the detection of Hg^{2+} in this study, the proposed biosensing strategy was in principle easy to extend to detect other targets (e.g. other metal ions or proteins) by replacing the T-Hg^{2+}-T complexes with other specificity structures that selectively bound the other targets. This biosensing strategy should be an alternative tool for the analysis of Hg^{2+} in environmental samples.

4. Conclusions

In this study, a portable EWOB was developed for simple, rapid, and sensitive on-site detection of Hg^{2+} using CY-A14 and BQ-T14 as signal reporter and biorecognition element, respectively. The influence of several key environmental factors on Hg^{2+} biosensor, such as pH, temperature, and ionic strength, was in details investigated in order to obtain optimal detection conditions. Under optimal conditions, a detection cycle for a single sample, including the measurement and regeneration, was under 10 min with a Hg^{2+} detection limit of 8.5 nM. The high selectivity of the biosensor was showed by evaluating its response to various potentially interfering metal ions. Our results clearly demonstrated that the portable EWOB could serve as a powerful tool for simple, rapid and sensitive on-site detection of Hg^{2+} in real water samples, and was potentially applicable to detect other heavy metal ions or small molecule targets for which DNA/aptamers could be applied as specific

Table 1
Detection results of water samples spiked with Hg^{2+}.

Origin	Hg^{2+} added to the samples (nM)	Hg^{2+} determined by biosensor (nM)	CV (%)	Recovery (%)
Tap water	75	73.6	4.0	98.2
	115	107.8	0.9	93.7
	185	194.9	3.1	105.4
Bottle water	75	78.3	3.9	104.4
	115	102.5	4.8	89.2
	185	193.7	3.5	104.7
	75	65.4	3.3	87.2
Lake water	115	91.8	4.4	79.8
	185	162.6	1.4	87.9
Underground water	75	83.5	3.3	111.4
	115	95.7	4.4	83.2
	185	176.8	1.4	95.6

The initial concentration of Hg^{2+} in all samples was undetectable (<2.1 nM). The reliability of data is expressed as coefficient of variation (CV, %; n = 3).

biosensing probes. The EWOB satisfies various key analytical parameters, such as high sensitivity and selectivity, portability, short assay time, easy-to-operation, cost-effectiveness and robustness, which is a long-standing unmet challenge for the detecting of heavy metal ions, especially for in field detection. Our ongoing work will be to develop an automated portable device to carry out parallel detection of multiple heavy metal ions using evanescent wave multicolor fluorescence technology.

CRediT authorship contribution statement

Yue Zhou: Methodology, Writing – original draft. **Hongliang Wang:** Formal analysis, Visualization. **Dan Song:** Data curation. **Zhanguo Li:** Investigation. **Shitong Han:** Resources. **Feng Long:** Conceptualization, Writing – review & editing. **Anna Zhu:** Conceptualization, Writing – review & editing.

Declaration of competing interest

The authors declare that they have no known competing financial interests or personal relationships that could have appeared to influence the work reported in this paper.

Acknowledgments

This research was financially supported by the National Natural Science Foundation of China (21675171), the Original Innovation Joint Fund of Beijing Natural Science Foundation-Haidian (L182045).

Appendix A. Supplementary data

Supplementary data to this article can be found online at https://doi.org/10.1016/j.aca.2021.338351.

References

[1] D.W. Domaille, E.L. Que, C.J. Chang, Synthetic fluorescent sensors for studying the cell biology of metals, Nat. Chem. Biol. 4 (2008) 168–175.
[2] E.M. Nolan, S.J. Lippard, Tools and tactics for the optical detection of mercuric ion, Chem. Rev. 108 (2008) 3443–3480.
[3] X.B. Zhang, R.M. Kong, Y. Lu, Metal ion sensors based on DNAzymes and related DNA molecules, Annu. Rev. Anal. Chem. 4 (2011) 105–128.
[4] J.L. Barringer, Z. Szabo, P.A. Reilly, Occurrence and mobility of mercury in groundwater: (Chapter 5), InTech2013.
[5] T. Kokab, A. Shah, F.J. Iftikhar, J. Nisar, M.S. Akhter, S.B. Khan, Amino acid-fabricated glassy carbon electrode for efficient simultaneous sensing of zinc(II), cadmium(II), copper(II), and mercury(II) ions, ACS Omega 4 (2019) 22057–22068.
[6] Q. Bao, G. Li, Z. Yang, P. Pan, J. Liu, J. Chang, J. Wei, L. Lin, Electrochemical performance of a three-layer electrode based on Bi nanoparticles, multi-walled carbon nanotube composites for simultaneous Hg(II) and Cu(II) detection, Chin. Chem. Lett. (2020).
[7] M. Natasha, S. Shahid, I. Khalid, J. Bibi, N. Bundschuh, Niazi Khan, C. Dumat, A critical review of mercury speciation, bioavailability, toxicity and detoxification in soil-plant environment: ecotoxicology and health risk assessment, Sci. Total Environ. 711 (2020), 134749.
[8] M.M. Kiy, A. Zaki, A.B. Menhaj, A. Samadi, J. Liu, Dissecting the effect of anions on Hg2+ detection using a FRET based DNA probe, The Analyst 137 (2012) 3535–3540.
[9] Q. Li, Z. Zhang, Z. Wang, Determination of Hg^{2+} by on-line separation and preconcentration with atmospheric-pressure solution-cathode glow discharge atomic emission spectrometry, Anal. Chim. Acta 845 (2014) 7–14.
[10] H. Luo, X. Wang, R. Dai, Y. Liu, X. Jiang, X. Xiong, K. Huang, Simultaneous determination of arsenic and cadmium by hydride generation atomic fluorescence spectrometry using magnetic zero-valent iron nanoparticles for separation and pre-concentration, Microchem. J. 133 (2017) 518–523.
[11] G. Maduraiveeran, M. Sasidharan, V. Ganesan, Electrochemical sensor and biosensor platforms based on advanced nanomaterials for biological and biomedical applications, Biosens. Bioelectron. 103 (2018) 113–129.
[12] T. Lech, W. Turek, Application of TDA AAS to direct mercury determination in postmortem material in forensic toxicology examinations, J. Anal. Toxicol. 43 (2019) 385–391.
[13] M. Ebrahimi, J.B. Raoof, R. Ojani, Sensitive electrochemical DNA-based biosensors for the determination of Ag^{+} and Hg^{2+} ions and their application in analysis of amalgam filling, J. Iran. Chem. Soc. 15 (2018) 1871–1880.
[14] B. Zhou, X.Y. Yang, Y.S. Wang, J.C. Yi, Z. Zeng, H. Zhang, Y.T. Chen, X.J. Hu, Q.L. Suo, Label-free fluorescent aptasensor of Cd^{2+} detection based on the conformational switching of aptamer probe and SYBR green I, Microchem. J. 144 (2019) 377–382.
[15] X. Li, Z. Du, S. Lin, J. Tian, H. Tian, W. Xu, ExoIII and TdT dependent isothermal amplification (ETDA) colorimetric biosensor for ultra-sensitive detection of Hg^{2+}, Food Chem. 316 (2020), 126303.
[16] A. Ono, H. Togashi, Highly selective oligonucleotide-based sensor for mercury(II) in aqueous solutions, Angew. Chem. 43 (2004) 4300–4302.
[17] S.H. Wu, B. Zhang, F.F. Wang, Z.Z. Mi, J.J. Sun, Heating enhanced sensitive and selective electrochemical detection of Hg^{2+} based on T-Hg^{2+}-T structure and exonuclease III-assisted target recycling amplification strategy at heated gold disk electrode, Biosens. Bioelectron. 104 (2018) 145–151.
[18] Y. Shan, B. Wang, H. Huang, D. Jian, X. Wu, L. Xue, S. Wang, F. Liu, On-site quantitative Hg^{2+} measurements based on selective and sensitive fluorescence biosensor and miniaturized smartphone fluorescence microscope, Biosens. Bioelectron. 132 (2019) 238–247.
[19] S.-P. Cao, H.-M. Hu, R.-P. Liang, J.-D. Qiu, An ultrasensitive electrochemiluminescence resonance energy transfer biosensor for divalent mercury monitoring, J. Electroanal. Chem. (2020) 856.
[20] Z. Li, H. Sun, X. Ma, R. Su, R. Sun, C. Yang, C. Sun, Label-free fluorescence "turn-on" strategy for mercury (II) detection based on the T-Hg^{2+}-T configuration and the DNA-sensitized luminescence of terbium (III), Anal. Chim. Acta 1099 (2020) 136–144.
[21] F. Long, M. He, A.N. Zhu, H.C. Shi, Portable optical immunosensor for highly sensitive detection of microcystin-LR in water samples, Biosens. Bioelectron. 24 (2009) 2346–2351.
[22] Chris R. Taitt, G.P. Anderson, F.S. Ligler, Evanescent wave fluorescence biosensors: advances of the last decade, Biosens. Bioelectron. 76 (2016) 103–112.
[23] T. van der Wijst, C. Fonseca Guerra, M. Swart, F.M. Bickelhaupt, B. Lippert, Rare tautomers of 1-methyluracil and 1-methylthymine: tuning relative stabilities through coordination to PtII complexes, Chem. Eur J. 15 (2009) 209–218.
[24] D. Zhou, L. Zeng, J. Pan, Q. Li, J. Chen, Autocatalytic DNA circuit for Hg^{2+} detection with high sensitivity and selectivity based on exonuclease III and G-quadruplex DNAzyme, Talanta 207 (2020), 120258.
[25] Y. Tanaka, S. Oda, H. Yamaguchi, Y. Kondo, C. Kojima, A. Ono, 15N-15N J-coupling across Hg(II): direct observation of Hg(II)-mediated T-T base pairs in a DNA duplex, J. Am. Chem. Soc. 129 (2007) 244–245.
[26] H. Torigoe, A. Ono, T. Kozasa, Hg(II) ion specifically binds with T:T mismatched

base pair in duplex DNA, Chem. Eur J. 16 (2010) 13218–13225.
[27] A. Ono, H. Torigoe, Y. Tanaka, I. Okamoto, Binding of metal ions by pyrimidine base pairs in DNA duplexes, Chem. Soc. Rev. 40 (2011) 5855–5866.
[28] H. Yamaguchi, J. Sebera, J. Kondo, S. Oda, T. Komuro, T. Kawamura, T. Dairaku, Y. Kondo, I. Okamoto, A. Ono, J.V. Burda, C. Kojima, V. Sychrovský, Y. Tanaka, The structure of metallo-DNA with consecutive thymine-HgII-thymine base pairs explains positive entropy for the metallo base pair formation, Nucleic Acids Res. 42 (2014) 4094–4099.
[29] I. Okamoto, K. Iwamoto, Y. Watanabe, Y. Miyake, A. Ono, Metal-ion selectivity of chemically modified uracil pairs in DNA duplexes, Angew. Chem. 48 (2009) 1648–1651.
[30] D. Peter, Nucleic Acid Hybridisation: A Practical Approach: edited by B. D. Hames and S. J. Higgins, IRL Press, 1985. , 1986.
[31] I. Kratochvílová, M. Golan, M. Vala, M. Špérová, M. Weiter, O. Páv, J. Šebera, I. Rosenberg, V. Sychrovský, Y. Tanaka, F.M. Bickelhaupt, Theoretical and experimental study of charge transfer through DNA: impact of mercury mediated T-Hg-T base pair, J. Phys. Chem. B 118 (2014) 5374–5381.
[32] E. Ozkumur, S. Ahn, A. Yalçin, C.A. Lopez, E. Cevik, R.J. Irani, C. DeLisi, M. Chiari, M.S. Unlü, Label-free microarray imaging for direct detection of DNA hybridization and single-nucleotide mismatches, Biosens. Bioelectron. 25 (2010) 1789–1795.
[33] M.M. Kiy, Z.E. Jacobi, J. Liu, Metal-induced specific and nonspecific oligonucleotide folding studied by FRET and related biophysical and bioanalytical implications, Chem. Eur J. 18 (2012) 1202–1208.
[34] Z. Zhan, X. Ma, C. Cao, S.J. Sim, Gold-based optical biosensor for single-mismatched DNA detection using salt-induced hybridization, Biosens. Bioelectron. 32 (2012) 127–132.
[35] J. Kang, J. Jung, S.K. Kim, Flexibility of single-stranded DNA measured by single-molecule FRET, Biophys. Chem. 195 (2014) 49–52.
[36] S. Rodriguez-Mozaz, M.J.L.d. Alda, M.-P. Marco, D. Barceló, Biosensors for environmental monitoring: a global perspective, Talanta 65 (2005) 291–297.